Revision_1

H-bonding scheme in allactite: A combined single-crystal neutron/X-ray diffraction, EPMA-WDS, FTIR and OAS study

Running title: H-bonding scheme in allactite

Corresponding author: G. Diego GATTA
Dipartimento di Scienze della Terra,
Università degli Studi di Milano,
Via Botticelli 23,
I-20133 Milano, Italy
Email: diego.gatta@unimi.it
Tel. : +39 02 503 15607
Fax: +39 02 503 15597

Submitted to Min. Mag.

H-bonding scheme in allactite: A combined single-crystal neutron/X-ray diffraction, EPMA-WDS, IR and OAS study

G. Diego Gatta[1,2], Ferdinando Bosi[3,4], Maria Teresa Fernandez Diaz[5], Ulf Hålenius[6]

[1] Dipartimento di Scienze della Terra, Università degli Studi di Milano, Via Botticelli 23, I-20133 Milano, Italy
[2]CNR - Istituto di Cristallografia, Sede di Bari, Via G. Amendola 122/o, I-70126 Bari, Italy
[3]Dipartimento di Scienze della Terra, Sapienza Università di Roma, Piazzale Aldo Moro 5, I-00185 Roma, Italy
[4]CNR-Istituto di Geoscienze e Georisorse, UOS Roma, P.le Aldo Moro 5, 00185 Roma, Italy
[5]Institut Laue-Langevin, BP 156, F-38042 Grenoble Cedex 9, France
[6]Department of Geosciences, Swedish Museum of Natural History, Box 50007, SE-10405 Stockholm, Sweden

Abstract

The crystal chemistry of allactite from Långban, Värmland (Sweden) was investigated by single-crystal X-ray and neutron diffraction, optical absorption spectroscopy, Fourier-transform infra-red spectroscopy (FTIR) and electron microprobe analysis by wavelength dispersive spectroscopy (EPMA-WDS). The optical spectra show indications for the presence of Mn in the valence state 2+ only. Assuming 16 O atoms per formula unit, arsenic as As^{5+} and the (OH) content calculated by charge balance, the resulting unit formula based on the EPMA-WDS data is $(Mn^{2+}_{6.73}Ca_{0.13}Mg_{0.12}Zn_{0.02})_{\Sigma 7.00}(As^{5+})_{2.00}O_{16}H_8$, very close to the ideal composition $Mn_7(AsO_4)_2(OH)_8$. In the unpolarised FTIR-spectrum of allactite, fundamental (OH)-stretching bands are observed at 3236, 3288, 3387, 3446, 3484, 3562 and 3570 cm^{-1}, suggesting that a number of (OH) environments, with different hydrogen bond strengths, occur in the structure. The neutron structure refinement shows that four independent H sites occur in allactite with full site occupancy, all as members of

hydroxyl groups. The complex hydrogen bonding scheme in the allactite structure is now well defined, with at least nine hydrogen bonds energetically favorable with mono-, bi- and tri-furcated configurations.

Keywords: allactite, arsenates, electron microprobe analysis, X-ray and neutron diffraction, optical absorption and infrared spectroscopy, hydrogen bonding.

Introduction

Allactite, ideally $Mn_7(AsO_4)_2(OH)_8$, is a member of the series of basic arsenates of manganese with general formula $Mn_n^{2+}(AsO_4)_z^{3-}(OH)^-_{2n-3z}$. This group of minerals occurs in low temperature hydrothermal vein systems, associated with manganese-iron oxide ore-bodies of the pyrometasomatic type in dolomitic marbles. There are only a few studies devoted to the mineralogy and crystal chemistry of allactite (Sjögren, 1884a, 1884b; Moore, 1968; Welin, 1968; Dunn 1983; Frost and Weier, 2006), likely due to the rarity of this mineral. Only a few occurrences are known worldwide: in veinlets through metamorphosed manganese deposits of the Moss and Brattfors mines, Nordmark (Sveden) and at Långban, Värmland (Sweden); in a metamorphosed stratiform zinc orebody at Franklin, Ogdensburg, Sussex Co., New Jersey (U.S.A.).

The crystal structure of allactite (from the type locality of Långban, in Sweden) was solved and refined to a crystallographic *R* factor of 0.077 by Moore (1968), on the basis of X-ray intensity data collected with a Weissenberg apparatus. Allactite structure was found to be monoclinic, with space group $P2_1/a$, unit-cell parameters a = 11.03(2) Å, b = 12.12(2) Å, c = 5.51(1) Å and β =114.07° (Z = 2), and a standard error on the refined bond distances of about ±0.03 Å. No further diffraction studies have so far been

devoted to this mineral. The structure is built up by bands of octahedra, two octahedra wide, held together by vertex-linked octahedra, forming flat sheets (parallel to (001) in Fig. 1). These sheets are, in turn, held together by chains of linked Mn-octahedra and As-tetrahedra running parallel to [010] (Fig. 1). The bridging Mn-octahedra connect to the sheets in a complicated fashion, exhibiting corner-, edge- and face-sharing with them (Fig. 1). Based on the data of Moore (1968), the four independent Mn-octahedra and the unique As-tetrahedron appear being significantly distorted. Despite the structure model reported by Moore (1968) appears being consistent, all the atomic sites were modelled as isotropic and no H-site was located, making unknown the H-bonding scheme in allactite. Based on bond valence arguments, Moore (1968) identified four O atoms belonging to the OH groups expected in the allactite structure.

Later, the crystal structure of raadeite, ideally $Mg_7(PO_4)_2(OH)_8$, was published by Chopin *et al*. (2001). The authors described the structure of raadeite in the space group $P2_1/n$ with a = 5.250(1) Å, b = 11.647(2) Å, c = 9.655(2) Å and β = 95.94(1)° (Z =2), recognizing the isostructural relation between raadeite and allactite and pointing out that Moore (1968) presented the allactite structure on a non-reduced cell. The reduced cell for allactite can be obtained from Moore's cell choice by the transformation [001/010/-10-1]. Consistently, the structure of argandite, ideally $Mn_7(VO_4)_2(OH)_8$ (the V analogue of allactite) was later reported by Brugger *et al*. (2011) in the space group $P2_1/n$ with a = 5.5038(2) Å, b = 12.2665(5) Å, c = 10.1055(5) Å and β = 95.559(4)° (Z = 2), and the isostructural relation with allactite and raadeite was revealed. In the structure refinements of raadeite and argandite, four independent H sites were located by inspection of the difference-Fourier map of the electron density. The proton sites were modelled isotropically and their positions were fixed (and not refined) in the raadeite refinement and refined in the argandite refinement.

115 Raman and infrared spectra of allactite from Nordmark (Sweden) were reported
116 by Frost and Weier (2006). Their infrared (ATR-IR) spectrum showed a very broad
117 spectral profile and, in addition, recording strong (OH)-stretching bands at very high
118 wave numbers (~3650 and ~3675 cm^{-1}). Frost and Weier (2006) assumed the distorted
119 spectrum profile to be due to adsorbed water. They suggested that the reason for
120 multiple bands in the (OH)-stretching region was caused by all "OH units" not being at
121 the same position in the structure, but offered no additional suggestions regarding the
122 hydrogen bonding in the mineral.

123 In order to obtain more precise structural and crystal chemical information, we
124 reinvestigated the crystal structure of allactite from the same locality as that previously
125 studied by Moore (1968) by single-crystal X-ray and neutron diffraction, optical
126 absorption spectroscopy, Fourier-transform infra-red spectroscopy (FTIR) and electron
127 microprobe analysis by wavelength dispersive spectroscopy (EPMA-WDS). The aim of
128 this study is to provide:

129 a) A crystal chemical characterization of this mineral, according to modern
130 standards;

131 b) An unambiguous location of all the proton sites and the description of the
132 complex H-bonding network expected for the allactite structure, along with its
133 low-*T* induced rearrangement;

134 c) The anisotropic displacement parameters of all the atomic sites, including the
135 H-sites;

136 d) The IR (OH)-stretching bands and their correlation with the H-bonding
137 scheme deduced on the basis of the neutron structure refinement.

138 As X-ray diffraction data did not allow to locate accurately the H atoms in the
139 allactite structure (Moore, 1968), single-crystal neutron diffraction represents the best

experimental technique to answer the open questions about the crystal structure/crystal chemistry of this hydrous Mn-arsenate. The high crystalline quality, the chemical homogeneity, and the size of the allactite crystals from Långban make this mineral an excellent sample for a single-crystal neutron diffraction study.

Sample description and mineralogy

The present allactite specimen (NRM #19140395), from the collections of the Swedish Natural History Museum in Stockholm, was collected at the beginning of the 20th century at the well-known Långban Mn-Fe oxide deposit in central Sweden (*e.g.*, Holtstam and Langhof, 1999). The specimen represents a ca. 15 cm thick allactite-rich late-stage vein that cuts the dolomite-hosted oxide ore. The purplish red colored allactite single crystals attain sizes of up to 15 mm and they frequently show tabular forms on {100}. Allactite coexists with native lead, calcite, dolomite, domeykite and pyrochroite.

Experimental methods

- Electron Microprobe Analysis

After X-ray investigation (see below), the same crystal of allactite was mounted on a glass slide, polished and carbon-coated for the EPMA-WDS analysis with a Cameca SX50 instrument at the "Istituto di Geologia Ambientale e Geoingegneria (Rome, Italy), CNR", operating at an accelerating potential of 15 kV and a sample current of 15 nA, 1 μm beam diameter. The following standards were used: wollastonite (Ca), olivine (Mg), rhodonite (Mn), sphalerite (Zn) and synthetic gallium arsenide (As). Wavelength dispersive scans revealed no detectable amounts of any additional elements. The PAP routine was applied (Pouchou and Pichoir, 1991). The results are listed in Table 1.

- **Single-crystal X-ray diffraction experiment**

A representative fragment of studied sample of allactite was selected for X-ray diffraction measurements on a Bruker KAPPA APEX-II single-crystal diffractometer, at Sapienza University of Rome (Earth Sciences Department), equipped with a CCD area detector (6.2 × 6.2 cm active detection area, 512 × 512 pixels) and a graphite crystal monochromator, using Mo$K\alpha$ radiation from a fine-focus sealed X-ray tube. The sample-to-detector distance was set to 4 cm. A total of 4708 exposures (step = 0.2°, time/step = 20 s), covering a full reciprocal sphere with a redundancy of 4, was used (Table 2). Final unit-cell parameters were refined using the Bruker AXS SAINT program for reflections with $I > 10\ \sigma(I)$ in the range $2.5° < \theta < 40°$ (Bruker, 2008; Table 2). The intensity data were processed and corrected for Lorentz, polarization, and background effects with the APEX2 software program of Bruker AXS (Bruker, 2008). The data were corrected for absorption using the multi-scan method (SADABS; Bruker, 2008). The absorption correction led to a significant improvement in R_{int}. The diffraction pattern was indexed with the reduced unit-cell reported in Table 2. The reflection conditions suggested the $P2_1/n$ space group.

- **Single-crystal neutron diffraction experiment**

A millimetric prismatic crystal of allactite (3.8 × 3.2 × 2.8 mm), free of defects under the polarised optical microscope, was selected for the neutron diffraction experiments. Neutron-diffraction data were measured at 293 K and at 100 K on the four-circle diffractometer D9, at the high-flux research reactor of the Institut Laue-Langevin (ILL) in Grenoble, France, with a neutron beam of wavelength 0.8370(2) Å, obtained by reflection from a Cu(220) monochromator. The D9 diffractometer is

equipped with a small two-dimensional area detector (Lehmann *et al.*, 1989), which allowed optimum resolution of the peaks from the background. Diffraction data were collected up θ_{max} of 34.6° and 32.6° at 293 K and 100 K, respectively (*h, k, l* ranges are listed in Table 2). For all data, background corrections following Wilkinson *et al.* (1988) and Lorentz corrections were applied. Absorption corrections were made by Gaussian integration (Coppens *et al*., 1965), using the calculated attenuation coefficient with account taken of the wavelength dependence of the absorption for the hydrogen content (Howard *et al*., 1987). Initial structural refinements showed that extinction affected only a few reflections, and could be well accounted for by the simple isotropic extinction model in SHELX-97 (Sheldrick, 2008). The low degree of extinction meant that the data for could be averaged over symmetry-equivalent reflections. Averaging in the 2/*m* Laue class of the 2222 (at 293 K) and 2063 (at 100 K) reflections scanned gave 1561 (at 293 K) and 1278 (at 100 K) unique reflections with an internal discrepancy index of 0.0403 (at 293 K) and 0.0255 (at 100 K). Since the three-dimensional count distribution around each reflection was observed, the centroids of all scanned reflections could be found. Least-squares matching of the observed and calculated centroids of a few hundreds of strongest reflections for the collections at 293 K and at 100 K gave the lattice constants listed in Table 2. The reflection conditions suggested the space group $P2_1/n$. Other details pertaining to the neutron data collections are listed in Table 2.

- **Optical absorption and Fourier-transform infra-red spectroscopy**

Polarized, optical absorption spectra at 293 K were recorded in the spectral range 270 - 1700 nm (37037 - 5882 cm^{-1}) on two 88 μm thick, doubly-sided polished platelets prepared from a single crystal of allactite. The two platelets represented the optical *XY* and *YZ* planes, respectively. The orientations of the platelets were confirmed

by optical microscopy using conoscopic imaging. The spectra were recorded at a spectral resolution of 1 nm using an AvaSpec-ULS2048X16 spectrometer (270-1060 nm) attached via a 400 µm UV optical fiber to a Zeiss Axiotron UV-microscope, and at a spectral resolution of 3 nm using an AvaSpec-NIR256-1.7TEC spectrometer (1060-1700 nm) attached via a 400 µm IR optical fiber to the same microscope. A 75 W Xenon arc lamp (270-1060 nm) and a 100 W halogen lamp (1060-1700 nm) served as illuminating sources and Zeiss Ultrafluar 10x lenses served as objective and condenser. A UV-quality Glan-Thompson prism with a working range from 250 to 2700 nm (40000 to 3704 cm^{-1}) was used as polarizer. The size of the circular measure aperture was 200 µm in diameter. The wavelength scale of the spectrometer was calibrated against Ho_2O_3-doped and Pr_2O_3/Nd_2O_3-doped standards (Hellma glass filters 666F1 and 666F7) with an accuracy better than 15 cm^{-1} in the wavelength range 300-1100 nm.

A pressed KBr disc mixed with ca. 1 mg of powdered allactite sample was measured by Fourier-transform infra-red absorption spectroscopy to characterize OH absorption bands in the wavenumber range 2000-5000 cm^{-1} using a Bruker Equinox 55 spectrometer equipped with a NIR source, a CaF_2 beam-splitter and an InSb detector. The unpolarized FTIR-spectrum was acquired during 256 cycles at a nominal spectral resolution of 4 cm^{-1}. Collected spectra were fitted using the Jandel PeakFit 4.12 software, assuming Gaussian peak shapes.

Results

- X-ray and neutron structure refinements

The anisotropic crystal-structure refinements based on the X-ray and neutron intensity data were performed using the SHELXL software (Sheldrick, 2008), starting

239 from the structure model of Moore (1968), but using the reduced cell choice reported by
240 Chopin *et al*. (2001) for raadeite (Table 2).

241 Variable parameters for the X-ray refinement were: scale factor, isotropic
242 extinction parameter, atom coordinates, atomic-displacement factors, and site-scattering
243 values expressed as mean atomic number (m.a.n.) for the *M1*, *M3* and *M4* sites (Table
244 3a). The refinement was conducted using neutral scattering factors (taken from the
245 *International Tables for Crystallography Vol. C*; Wilson and Prince, 1999), and
246 modelling the octahedrally coordinated sites *M1*, *M2*, *M3* and *M4* with Mn, the
247 tetrahedrally coordinated site with As, the anion sites with O. The *M2*, *As* and anion
248 sites were modelled with a fixed occupancy of 1, because refinement with
249 unconstrained occupancies showed no significant deviations from this value. Four
250 independent H sites were located by inspections of the maxima in the difference-Fourier
251 map; their position was then refined, but fixing the displacement parameters (Table 3a).
252 With this structure model, convergence was rapidly achieved and the variance-
253 covariance matrix showed no significant correlations between the refined parameters.
254 Further details pertaining to the structure refinements are given in Table 2; fractional
255 atomic coordinates, site occupancy and m.a.n., and displacement parameters are listed in
256 Table 3a; Table 4 shows selected bond distances. The calculated density is 3.856 g/cm^3.

257 The neutron refinements (at 293 and 100 K) were conducted with the neutron
258 scattering lengths of Mn, As, O and H according to Sears (1986). Correction for
259 secondary isotropic extinction was performed according to the protocol of Larson
260 (1967). The refinements were conducted with the scattering length of manganese at the
261 *M1*, *M2*, *M3* and *M4* sites, the length of arsenic at the *As* site and that of oxygen at the
262 eight independent O sites (*i.e*., *O1-8*) (Tables 3b and 3c). The first cycles of refinements
263 were conducted without any H sites. When convergence was achieved, the difference-

Fourier maps of the nuclear density showed four independent negative residuals, at ~1 Å from the *O1*, *O3*, *O5* and *O6* site, respectively. The structure model was then implemented with four additional sites occupied by hydrogen (here labelled as *H1*, *H3*, *H5* and *H6*, Tables 3b and 3c), as hydrogen has a negative neutron scattering length [(b_c(H) = –3.7409 fm; Sears, 1986]. All the sites showed no significant deviation from the full occupancy. With such a structure model, convergence was rapidly achieved and the variance-covariance matrix showed no significant correlation among the refined parameters. At the end of the last cycles of the refinement, no peaks larger than ±0.8 fm/Å^3 were present in the final difference-Fourier map of the nuclear density (Table 2). The final statistical index R_1 was 0.0421 (at 293 K) and 0.0331 (at 100 K) for 152 refined parameters and 1362 (at 293 K) and 1160 (at 100 K) unique reflections with Fo > 4σ(Fo) (Table 2). Site coordinates and displacement parameters are given in Tables 3b and 3c, relevant bond lengths and angles in Table 4. CIFs are deposited.

- **Optical and FTIR spectroscopy**

The recorded polarized optical absorption spectra (Fig. 2) show a set of sharp to moderately sharp electronic *d-d* bands typical for Mn^{2+} in oxygen-based minerals (*e.g.*, Burns, 1993; Hålenius *et al*., 2007). The molar absorption coefficient (ε) of the bands ranges up to 1.0 Lmol^{-1}cm^{-1}, which suggests that they may be related to electronic transitions in Mn^{2+} cation pairs in edge- or face-sharing octahedra (Lohr and McClure, 1968). In view of the structure of allactite that displays edge-sharing octahedra, this is not surprising. The energies of the recorded absorption bands and their assignments are summarized in Table 5. The tentative band assignments are based on the present crystal structure information for allactite and on the relationship between the energies of the $^6A_1(S) \rightarrow {}^4E_g(D)$ and $^6A_1(S) \rightarrow {}^4E_g{}^4A_{1g}(G)$ bands in octahedrally and tetrahedrally

coordinated Mn^{2+} observed in a large set of minerals and inorganic substances (*e.g.*, Hålenius *et al.*, 2007). The proposed assignments result in very reasonable Racah *B*- and *C*-parameters as well as crystal field splitting parameter, 10*Dq*, typical for octahedrally coordinated Mn^{2+}. A slightly higher 10*Dq* calculated for Mn^{2+} at the *M2*, *M3* and *M4* sites in relation to the value for Mn^{2+} at the *M1* site reflects that the *M1* site is coordinated by 4 O^{2-} and 2 $(OH)^{-}$, while the remaining *M2-4* sites are coordinated by 2 O^{2-} and 4 $(OH)^{-}$ (Table 4). The present optical spectra show no indications for a presence of other Mn valence states, as, *e.g.*, Mn^{3+}, in the sample.

In addition to the spin-forbidden electronic Mn^{2+} *d-d* bands, overtones of (OH)-stretching modes are recorded in the NIR-spectra at 6950 and 6965 cm^{-1}. In the unpolarised FTIR-spectrum of allactite (Fig. 3), fundamental (OH)-stretching bands are observed at 3236, 3288, 3387, 3446, 3484, 3562 and 3570 cm^{-1}. In contrast to the infrared spectrum of allactite published by Frost and Weir (2006), our IR-spectrum shows narrow and well defined stretching bands and their recorded bands at ~3650 and ~3675 cm^{-1} do not reproduce. Our spectrum demonstrates that a number of (OH) environments, with different hydrogen bond strengths, occur in allactite structure. Based on observed relationships between O···H distances as determined by diffraction studies and (OH)-stretching band energies (Libowitzky, 1999), the observed (OH)-stretching bands in the spectrum of allactite suggest that O···H distances in the mineral range from ~1.81 Å to ~2.21Å. The infrared spectra of the isostructural minerals raadeite $[Mg_7(PO_4)_2(OH)_8]$ and argandite $[Mg_7(PO_4)_2(OH)_8]$ show OH stretching bands in comparable spectral ranges (Chopin *et al.* 2001; Brugger *et al.*, 2011).

Discussion

The EPMA-WDS data of the allactite sample from Långban confirm the previous experimental findings of Moore (1968). The atomic proportions were calculated assuming that the valence state of Mn is 2+, as indicated by optical spectroscopic information (see below), and the valence state of As is 5+ on the basis of the allactite stoichiometry (Table 1). Assuming 16 O atoms per formula unit (*a.p.f.u.*), and the (OH)-content calculated by charge balance, the resulting unit formula is

$$(Mn^{2+}_{6.73}Ca_{0.13}Mg_{0.12}Zn_{0.02})_{\Sigma 7.00}(As^{5+})_{2.00}O_{16}H_8,$$

very close to the end-member composition $Mn_7(AsO_4)_2(OH)_8$. The X-ray and neutron structure refinements corroborate the crystal chemistry of allactite, and the site populations at the octahedrally coordinated sites *M1*, *M2*, *M3* and *M4*, modelled following the protocol of Wright *et al.* (2000) and using the X-ray structural data, leads to the following structural formula:

$$^{M1}(Mn^{2+}_{0.85}Ca_{0.13}Zn_{0.02})_{\Sigma 1.00}{}^{M2}(Mn^{2+}_{2.00})^{M3}(Mn^{2+}_{1.95}Mg_{0.05})_{\Sigma 2.00}{}^{M4}(Mn^{2+}_{1.92}Mg_{0.08})_{\Sigma 2.00}$$
$$(AsO_4)_2(OH)_8.$$

There is an excellent match between the number of electrons per formula unit (*e.p.f.u.*) derived on the basis of the EPMA-WDS data and those obtained by the X-ray structure refinement: 238.8 and 238.7 *e.p.f.u.*, respectively.

There is a slight difference in the lengths of unit-cell edges obtained by X-ray and neutron diffraction data collected at 293 K (with a difference in the unit-cell volume by 2.8%, Table 2), which is reflected by the refined intra-polyhedral bond distances as well (Table 4). This difference can be ascribed to the different techniques used, if we consider the sample of allactite as chemically homogeneous. However, we cannot exclude a slightly different chemical composition of the crystals used for the X-ray and neutron diffraction experiments, respectively.

X-ray and neutron structure refinements lead to a general structure model in agreement with that of Moore (1968), but much more precise with standard errors on bond distances smaller than 0.001 Å and location of the H atoms (Table 4). The structure of allactite is built up by sheets of octahedra (two octahedra wide and held together by vertex-linked octahedra) parallel to (001) (Fig. 1). These sheets are, in turn, held together by chains of linked Mn-octahedra and As-tetrahedra, running parallel to [010]. The bridging Mn-octahedra exhibit corner-, edge- and face-sharing connections (Fig. 1). The four independent Mn-octahedra are significantly distorted, but differently, as suggested by the difference between the longest and the shortest Mn-O bond lengths (*i.e.*, Δ_{max}) are $\Delta(M1)_{max} \approx 0.13$ Å, $\Delta(M2)_{max} \approx 0.48$ Å, $\Delta(M3)_{max} \approx 0.16$ Å, $\Delta(M4)_{max} \approx 0.20$ Å (neutron refinement based on data collected at 293 K, Table 4). The polyhedron coordinated by As^{5+} is less distorted, with $\Delta(As)_{max} \approx 0.04$ Å. To best quantify relative deviations from the average polyhedral bond length, the bond-length distortion parameters (Δ_{msda}: mean-square relative deviation from the average, Brown and Shannon, 1973) were calculated using X-ray structure model: $\Delta_{msda}(M1) = 0.0005$, $\Delta_{msda}(M2) = 0.0061$, $\Delta_{msda}(M3) = 0.0006$, $\Delta_{msda}(M4) = 0.0014$ and $\Delta_{msda}(As) = 0.0001$. Consistently with the neutron structure data, the X-ray data show that the most distorted octahedra is *M2*, followed by *M4* and then by *M3* and *M1*.

The neutron structure refinements show that four independent H sites occur in the structure of allactite with full site occupancy (*i.e.*, *H1*, *H3*, *H5* and *H6*, Tables 3b and 3c), all as member of hydroxyl groups of the structure (*i.e.*, *O1-H1*, *O3-H3*, *O5-H5*, *O6-H6*, Table 4). This experimental finding is in line with the previous studies on raadeite (Chopin *et al.*, 2001) and argandite (Brugger *et al.*, 2011). The principal root-mean-square components of the H-sites displacement parameters obtained in this study are fairly anisotropic (as deducible from the data reported in Tables 3b and 3c). The O-H

bond distances corrected for "riding motion" effects are listed in Table 4. The complex hydrogen bonding scheme in allactite structure is now well defined with at least nine different hydrogen bonds energetically favorable (Fig. 4, Table 4) with:

- *O1* as *donor* and *O8* as *acceptor* (with *H1···O8* = 1.888(3) Å, *O1···O8* = 2.854(3) Å and *O1-H1···O8* = 172.0(2)° at 293 K, Fig. 4, Table 4*)*;
- *O3* as *donor* and *O5, O6* and *O8* as *acceptors*, with a tri-furcated configuration (with *H3···O5* = 2.695(3) Å and *O3-H3···O5* = 111.2(2)°, *H3···O6* = 2.822(3) Å and *O3-H3···O6* = 151.2(2)°, and *H3···O7* = 2.900(3) Å and *O3-H3···O7* = 132.1(2)° at 293 K, Fig. 4, Table 4);
- *O5* as *donor* and *O3, O7* and *O8* as *acceptors*, with a tri-furcated configuration (with *H5···O8* = 2.098(3) Å and *O5-H5···O8* = 159.9(2)°, *H5···O7* = 2.553(3) Å and *O5-H5···O7* = 114.4(2)°, and *H5···O3* = 2.615(3) Å and *O5-H5···O3* = 116.8(2)° at 293 K, Fig. 4, Table 4);
- *O6* as *donor* and *O4* and *O8* as *acceptors*, with a bi-furcated configuration (with *H6···O8* = 2.197(3) Å and *O6-H6···O8* = 154.3(2)°, and *H6···O4* = 2.587(3) Å and *O6-H6···O4* = 135.1(2)° at 293 K, Fig. 4, Table 4).

The strongest H-bond of the structure involves *O1* as *donor* and *O8* as *acceptor*. All the others are comparably weaker (and weak in general), and reflect the bi- or tri-furcated configurations previously described. The described H-bonding scheme is kept at low temperature (Table 4). As expected, the magnitude of the atomic displacement ellipsoids (here described in the expression: $-2\pi^2[(ha^*)^2U^{11} + \ldots + 2hka^*b^*U^{12} + \ldots + 2klb^*c^*U^{23}]$) is (on the average) reduced by 30% at 100 K, if compared to the values refined at 293 K (Tables 3b and 3c). The unambiguous location of all the H sites in the structure of allactite shows that there are two types of octahedral building units of

389 the structure: $^{M1}MO_4(OH)_2$ and $^{M2,M3,M4}MO_2(OH)_4$; no MO_6 unit occurs, consistently
390 with the previous findings on raadeite (Chopin *et al*., 2001) and argandite (Brugger *et*
391 *al*., 2011). The optical absorption experiment of this study confirms that the Mn valence
392 state is 2+, and no evidence of partial substitution with *e.g.* Mn^{3+} is observed.

393 In the unpolarised FTIR-spectrum of allactite (Fig. 3), at least seven (OH)-
394 stretching bands can be distinctly observed (at 3236, 3288, 3387, 3446, 3484, 3562 and
395 3570 cm^{-1}). This finding suggests that several (OH) environments occur, with different
396 hydrogen-bond strengths. Applying the protocol of Libowitzky (1999), based on
397 observed correlation between O···H distances and (OH)-stretching band energies, the
398 recorded (OH) bands of this study suggest that O···H distances in the structure of
399 allactite range at least from ~1.81 Å to ~2.21 Å. Due to a very small slope of the
400 correlation curve for weaker (longer) hydrogen bonds, the indicated upper limit for
401 O···H distances is highly uncertain. For O···H distances in the range 2.3 to 3.0 Å, the
402 related (OH)-stretching bands are predicted to occur within a narrow frequency range of
403 merely ~40 cm^{-1}. Infrared spectra of substances with several different hydrogen bonds
404 with O···H distances longer than 2.3 Å, as in allactite, will consequently show
405 considerable overlaps, and bands related to different (OH) environments may not be
406 fully resolved. In addition, it should be pointed out that the correlation curve published
407 by Libowitzky (1999) is mainly based on literature data on O···H distances deduced by
408 X-ray diffraction data, which are known to result in less accurate determinations of H
409 atom positions. Consequently, the correlation curve may be subject to systematic errors.
410 Taking the aforementioned uncertainties into account, one may conclude that FTIR
411 spectra demonstrate the existence of at least seven different O···H bonds with distances
412 larger than 1.82 Å in allactite. The neutron structure refinements corroborate FTIR data
413 and their interpretation, with nine independent H-bonds and O···H distances ranging

between ~1.88 Å and ~2.90 Å (Table 4). It is interesting to note that the infrared spectra of the isostructural minerals raadeite [$Mg_7(PO_4)_2(OH)_8$] and argandite [$Mg_7(PO_4)_2(OH)_8$] show (OH)-stretching bands in comparable spectral ranges (Chopin *et al.* 2001; Brugger *et al*., 2011).

Acknowledgements

The authors thank the Institut Laue-Langevin (Grenoble, France), for the allocation of neutron beam time. Chemical analyses were performed with the kind assistance of M. Serracino, to whom the authors express their gratitude. Mark Cooper and an anonymous reviewers are thanked.

References

Bruker (2008) *APEX2*, *SAINT* and *SADABS,* Bruker AXS Inc., Madison, Wisconsin, USA.

Burns, R.G. (1993) *Mineralogical Applications of Crystal Field Theory* (2nd edition), p. 551, Cambridge University Press, Cambridge, U.K.

Busing, W.R. and Levy, H.A. (1964) The effect of thermal motion on the estimation of bond lengths from diffraction measurements. *Acta Crystallographica*, **17**, 142-146.

Brown, I.D. and Shannon, R.D. (1973) Empirical bond-strength-bond-length curves for oxide. *Acta Crystallographica*, A**29**, 266–282.

Brugger, J., Elliott, P., Meisser, N., and Ansermet, S. (2011) Argandite, $Mn_7(VO_4)_2(OH)_8$, the V analogue of allactite from the metamorphosed Mn ores at Pipji, Turtmann Valley, Switzerland. *American Mineralogist*, **96**, 1894–1900.

Chopin, C., Ferraris, G., Prencipe, M., Brunet, F., and Medenbach, O. (2001) Raadeite, $Mg_7(PO_4)_2(OH)_8$: a new dense-packed phosphate from Modum (Norway). *European Journal of Mineralogy*, **13**, 319-327.

Coppens, P., Leiserowitz, L., and Rabinovich, D. (1965) Calculation of absorption corrections for camera and diffractometer data. *Acta Crystallographica,* **18**, 1035-1038.

449 Dunn, P.J. (1983) Allactite from Franklin and Sterling Hill, New Jersey.
450 *Mineralogical Record*, **14**, 251–252.
451 Frost, R.L. and Weier, M. (2006) Raman and infrared spectroscopy of the
452 manganese arsenate mineral allactite. *Spectrochimica Acta, Part A: Molecular and*
453 *Biomolecular Spectroscopy*, **65A**, 623-627.
454 Hålenius, U., Bosi, F., and Skogby, H. (2007) Galaxite, $MnAl_2O_4$, a spectroscopic
455 standard for tetrahedrally coordinated Mn^{2+} in oxygen-based mineral structures.
456 *American Mineralogist*, **92**, 1225–1231.
457 Holtstam, D. and Langhof, J. (eds.) (1999) Långban, the mines, their minerals,
458 history and explorers. Raster Förlag, Stockholm, p. 215.
459 Howard, J.A.K., Johnson, O., Schultz, A.J., and Stringer, A.M. (1987)
460 Determination of the neutron absorption cross section for hydrogen as a function of
461 wavelength with a pulsed neutron source. *Journal of Applied Crystallography*, **20**, 120-
462 122.
463 Lehmann, M. S., Kuhs, W., McIntyre, G.J., Wilkinson, C., and Allibon, J. (1989)
464 On the use of a small two-dimensional position-sensitive detector in neutron diffraction.
465 *Journal of Applied Crystallography*, **22**, 562-568.
466 Libowitzky, E. (1999) Correlation of O-H stretching frequencies and O-H···O
467 hydrogen bond lengths in minerals. *Monatshefte für Chemie*, **130**, 1047–1059.
468 Lohr, L.L. and McClure, D.S. (1968) Optical spectra of divalent manganese salts
469 II. The effect of interionic coupling on absorption strength. *Journal of Chemical*
470 *Physics*, **49**, 3516–3521.
471 Moore, P.B. (1968) Crystal chemistry of the basic manganese arsenate minerals:
472 II. The crystal structure of allactite. *American Mineralogist*, **53**, 733–741.

Pouchou, J.L., and Pichoir, F. (1984) A new model for quantitative X-ray microanalysis. I. Application to the analysis of homogeneous samples. *La Recherche Aérospatiale*, **3**, 13–36.

Sears, V.F. (1986) Neutron Scattering Lengths and Cross-Sections. In K. Sköld and D.L. Price, Eds., Neutron Scattering, Methods of Experimental Physics, Vol. 23A, 521-550. Academic Press, New York.

Sheldrick, G.M. (2008) A short history of *SHELX*. *Acta Crystallographica*, **A64**, 112-122.

Sjögren, A. (1884a) Allaktit, ett nytt manganarseniat från Mossgrufvan å Nordmarksfältet. *Geologiska Föreningens i Stockholm Förhandlingar*, **7**, 109-111.

Sjögren, A. (1884b) Kristallografiska studier: VII Allaktit från Nordmarken. *Geologiska Föreningens i Stockholm Förhandlingar*, **7**, 220-236.

Welin, E. (1968) Notes on the mineralogy of Sweden 6. X-ray powder data for minerals from Långban and the related mineral deposits of Central Sweden. *Arkiv för Mineralogi och Geologi*, **4(30)**, 499-541.

Wilkinson, C., Khamis, H.W., Stansfield., R.F.D., and McIntyre, G.J. (1988) Integration of single-crystal reflections using area multidetectors. *Journal of Applied Crystallography*, **21**, 471-478.

Wilson, A.J.C. and Prince, E. (1999) *International Tables for Crystallography Vol. C, Mathematical, Physical and Chemical Tables*, second ed., Kluwer, Dordrecht.

Wright, S.E., Foley, J.A., and Hughes, J.M. (2000) Optimization of site occupancies in minerals using quadratic programming. *American Mineralogist*, **85**, 524–531.

498 Table 1. Chemical composition of allactite based on EPMA-WDS.

	wt%		*a.p.f.u.*
As_2O_5	28.8(4)	As^{5+}	2.00
MnO	59.8(5)	Mn^{2+}	6.73
MgO	0.61(3)	Mg	0.12
ZnO	0.17(7)	Zn	0.02
CaO	0.88(3)	Ca	0.13
H_2O[a]	9.03	OH	8.00
Total	99.34		

Note: Number of atoms calculated on basis of 16 oxygen atoms; estimated standard deviations in bracket; *a.p.f.u*. = atoms per formula unit.

[a] Calculated by stoichiometry.

499
500

501 Table 2. Details of X-ray and neutron data collections and refinements of allactite.
502
503
504

T (K)	293	293	100
Crystal shape	Prismatic	Prismatic	Prismatic
Crystal size (mm)	$0.28 \times 0.26 \times 0.25$	3.8 x 3.2 x 2.8	3.8 x 3.2 x 2.8
Crystal colour	Purplish red	Purplish red	Purplish red
Unit-cell constants (Å, °)	a = 5.5225(1)	a = 5.482(1)	a = 5.4786(8)
	b = 12.2760(3)	b = 12.153(2)	b = 12.156(2)
	c = 10.1230(2)	c = 10.014(2)	c = 10.008(1)
	β = 95.632(1)	β = 95.55(1)	β = 95.574(8)
Reference formula	$Mn_7(AsO_4)_2(OH)_8$	$Mn_7(AsO_4)_2(OH)_8$	$Mn_7(AsO_4)_2(OH)_8$
Space group	$P2_1/n$	$P2_1/n$	$P2_1/n$
Z	2	2	2
Radiation	Monochromatic, X-ray	Monochromatic, neutron	Monochromatic, neutron
Diffractometer	Bruker KAPPA APEX-II	D9 ILL	D9 ILL
λ (Å)	Mo$K\alpha$	0.8370	0.8370
θ_{max}(Å)	40.0	34.6	32.6
	$-9 \le h \le 8$	$-7 \le h \le 2$	$-6 \le h \le 2$
	$-21 \le k \le 21$	$-13 \le k \le 16$	$-12 \le k \le 15$
	$-18 \le l \le 18$	$-12 \le l \le 13$	$-11 \le l \le 12$
No. measured reflections	17817	2222	2063
No. unique reflections	3916	1561	1278
No. unique refl. with $F_o > 4\sigma(F_o)$	3632	1362	1160
No. refined parameters	131	152	152
R_{int}	0.0205	0.0403	0.0255
R_1 *(F)* with $F_o > 4\sigma(F_o)$	0.0173	0.0421	0.0331
R_1 *(F)* for all the unique reflections	0.0195	0.0501	0.0388
wR_2 *(F²)*	0.0423	0.0858	0.0622
Residuals (*e*-/ Å^3, fm/Å^3)	-0.55/+0.60	-0.66/+0.82	-0.42/+0.46

Notes: $R_{int} = \Sigma \mid F_{obs}^2 - F_{obs}^2(\text{mean}) \mid / \Sigma [F_{obs}^2]$; $R_1 = \Sigma||F_{obs}| - |F_{calc}||/\Sigma|F_{obs}|$; $wR_2 = [\Sigma[w(F^2_{obs} - F^2_{calc})^2]/\Sigma[w(F^2_{obs})^2]]^{0.5}$, $w = 1/[\sigma^2(F_{obs}^2) + (aP)^2 + bP]$, $P = (\text{Max}(F_{obs}^2, 0)+2F_{calc}^2)/3$. Refined extinction coefficient (as implemented in Shelx): 0.0080(3) for X-ray data, 0.061(2) for neutron data at 293 K.

505
506
507
508
509
510
511
512
513
514
515
516
517
518

Table 3a. Atomic coordinates and displacement parameters (Å^2) in the expression: $-2\pi^2[(ha^*)^2U^{11} + \ldots + 2hka^*b^*U^{12} + \ldots + 2klb^*c^*U^{23}]$, based on the X-ray structure refinement at 293 K. U_{eq} is defined as one third of the trace of the orthogonalised U^{ij} tensor. The site occupancy factor is 1 for As, O and H sites.

Site	*x*	*y*	*z*	$U_{eq/iso}$	U^{11}	U^{22}	U^{33}	U^{23}	U^{13}	U^{12}
M1	0	0	0	0.01198(6)	0.01383(12)	0.01089(9)	0.01118(9)	-0.00069(6)	0.00101(7)	-0.00116(7)
M2	0.26943(3)	0.18010(2)	0.20916(2)	0.01325(4)	0.01298(8)	0.01242(6)	0.01383(7)	-0.00170(5)	-0.00137(5)	0.00114(5)
M3	0.25119(3)	0.43095(2)	0.99254(2)	0.01153(5)	0.00931(9)	0.01120(7)	0.01390(7)	-0.00007(5)	0.00028(5)	-0.00052(4)
M4	0.24882(3)	0.21051(2)	0.50019(2)	0.01188(5)	0.01160(9)	0.01186(7)	0.01219(7)	0.00092(5)	0.00129(5)	-0.00035(5)
As	0.03424(2)	0.57922(2)	0.70814(2)	0.00843(3)	0.00802(5)	0.00823(4)	0.00895(4)	-0.00013(3)	0.00034(3)	0.00000(3)
O1	0.44857(16)	0.30618(6)	0.11469(8)	0.01301(13)	0.0129(4)	0.0133(3)	0.0128(3)	0.0006(2)	0.0014(2)	-0.0001(2)
O2	0.05926(15)	0.57025(6)	0.87826(8)	0.01133(12)	0.0116(3)	0.0128(3)	0.0094(3)	0.0006(2)	0.0001(2)	0.0003(2)
O3	0.07435(16)	0.84594(7)	0.90412(8)	0.01427(13)	0.0130(4)	0.0139(3)	0.0157(3)	0.0012(2)	0.0007(3)	0.0011(2)
O4	0.91527(17)	0.70196(6)	0.66775(8)	0.01638(15)	0.0232(4)	0.0112(3)	0.0143(3)	0.0018(2)	-0.0002(3)	0.0059(3)
O5	0.07742(16)	0.06280(6)	0.38765(8)	0.01345(13)	0.0124(4)	0.0118(3)	0.0160(3)	-0.0006(2)	0.0006(3)	-0.0003(2)
O6	0.54268(16)	0.18377(6)	0.37529(8)	0.01337(13)	0.0112(3)	0.0130(3)	0.0155(3)	0.0029(2)	-0.0007(3)	-0.0012(2)
O7	0.85266(16)	0.47996(7)	0.63903(8)	0.01462(14)	0.0157(4)	0.0126(3)	0.0147(3)	0.0004(2)	-0.0027(3)	-0.0050(2)
O8	0.32017(16)	0.57296(7)	0.66451(9)	0.01628(15)	0.0096(4)	0.0236(4)	0.0160(3)	-0.0046(3)	0.0030(3)	-0.0007(3)
H1	0.512(3)	0.3450(14)	0.1886(15)	0.016						
H3	0.179(3)	0.8674(15)	0.8498(16)	0.017						
H5	0.029(3)	0.0252(14)	0.3160(15)	0.016						
H6	0.626(3)	0.2478(12)	0.3673(17)	0.016						

Notes: s.o.f.(*M1*) = 0.979(1); *s.o.f.*(*M2*) = 1; *s.o.f.*(*M3*) = 0.986(1); *s.o.f.*(*M4*) = 0.979(1); Equivalent (U_{eq}) and isotropic (U_{iso}) displacement parameters; *H1,3,5,6* sites were constrained to have a $U_{iso} = 1.2\ U_{eq}$ of the co-respective *O1,3,5,6* sites.

Table 3b. Atomic coordinates and displacement parameters (Å^2) in the expression: $-2\pi^2[(ha^*)^2U^{11} + \ldots + 2hka^*b^*U^{12} + \ldots + 2klb^*c^*U^{23}]$, based on the neutron structure refinement at 293 K. U_{eq} is defined as one third of the trace of the orthogonalised U^{ij} tensor. The site occupancy factor is 1 for all the sites.

Site	*x*	*y*	*z*	U_{eq}	U^{11}	U^{22}	U^{33}	U^{23}	U^{13}	U^{12}
M1	0	0	0	0.0119(5)	0.0135(13)	0.0114(12)	0.0108(11)	-0.0004(9)	0.0016(10)	0.0001(9)
M2	0.2686(4)	0.1796(1)	0.2091(2)	0.0115(4)	0.0148(9)	0.0096(8)	0.0097(8)	-0.0023(6)	-0.0014(7)	0.0009(7)
M3	0.2516(4)	0.4306(2)	0.9923(3)	0.0160(4)	0.0170(10)	0.0155(9)	0.0154(9)	-0.0004(7)	0.0004(8)	-0.0001(9)
M4	0.2478(4)	0.2108(2)	0.5007(2)	0.0168(4)	0.0200(10)	0.0150(9)	0.0155(9)	0.0014(7)	0.0017(8)	-0.0006(8)
As	0.0340(2)	0.57939(8)	0.70777(9)	0.0068(2)	0.0085(5)	0.0053(4)	0.0064(4)	-0.0001(3)	-0.0002(4)	0.0001(4)
O1	0.4489(2)	0.3060(1)	0.1147(1)	0.0117(3)	0.0141(6)	0.0112(5)	0.0096(5)	-0.0001(4)	-0.0002(5)	-0.0005(5)
O2	0.0599(2)	0.5702(1)	0.8780(1)	0.0100(2)	0.0131(6)	0.0108(5)	0.0060(5)	0.0005(4)	0.0001(4)	0.0009(5)
O3	0.0756(2)	0.8466(1)	0.9048(1)	0.0118(3)	0.0124(6)	0.0107(5)	0.0117(5)	-0.0001(4)	-0.0014(5)	0.0015(5)
O4	0.9170(3)	0.7023(1)	0.6678(1)	0.0139(3)	0.0217(7)	0.0093(5)	0.0102(5)	0.0003(4)	-0.0009(5)	0.0046(5)
O5	0.5771(2)	0.4375(1)	0.8870(1)	0.0121(3)	0.0134(6)	0.0100(5)	0.0127(6)	0.0009(4)	0.0007(5)	0.0006(5)
O6	0.5425(2)	0.1838(1)	0.3751(1)	0.0118(3)	0.0118(6)	0.0115(6)	0.0119(5)	0.0022(4)	-0.0008(4)	-0.0014(5)
O7	0.8516(3)	0.4805(1)	0.6390(1)	0.0128(3)	0.0178(7)	0.0089(5)	0.0108(5)	0.0001(4)	-0.0034(5)	-0.0039(5)
O8	0.3203(2)	0.5726(1)	0.6640(1)	0.0147(3)	0.0118(6)	0.0215(6)	0.0111(5)	-0.0053(5)	0.0022(5)	-0.0018(5)
H1	0.5129(5)	0.3473(2)	0.1935(2)	0.0236(5)	0.0296(13)	0.0237(11)	0.0170(10)	-0.0047(9)	0.0001(9)	-0.0020(10)
H3	0.1805(6)	0.8674(2)	0.8399(3)	0.0350(6)	0.0347(15)	0.0384(15)	0.0342(14)	0.0130(12)	0.0153(12)	0.0026(12)
H5	0.5257(6)	0.4731(2)	0.8045(2)	0.0299(6)	0.0472(16)	0.0272(12)	0.0145(10)	0.0031(9)	-0.0017(10)	0.0011(11)
H6	0.6352(5)	0.2504(2)	0.3711(2)	0.0295(6)	0.0318(14)	0.0259(13)	0.0299(12)	0.0068(10)	-0.0017(10)	-0.0116(12)

Table 3c. Atomic coordinates and displacement parameters (Å^2) in the expression: $-2\pi^2[(ha^*)^2U^{11} + \ldots + 2hka^*b^*U^{12} + \ldots + 2klb^*c^*U^{23}]$, based on the neutron structure refinement at 100 K. U_{eq} is defined as one third of the trace of the orthogonalised U^{ij} tensor. The site occupancy factor is 1 for all the sites.

Site	*x*	*y*	*z*	U_{eq}	U^{11}	U^{22}	U^{33}	U^{23}	U^{13}	U^{12}
M1	0	0	0	0.0081(5)	0.0116(13)	0.0065(11)	0.0061(10)	0.0001(9)	0.0006(9)	-0.0007(9)
M2	0.2683(3)	0.1796(1)	0.2094(2)	0.0063(3)	0.0073(9)	0.0050(7)	0.0064(7)	-0.0012(6)	-0.0007(6)	-0.0003(7)
M3	0.2513(3)	0.4310(2)	0.9930(2)	0.0120(4)	0.0136(7)	0.0101(8)	0.0123(8)	0.0005(7)	0.0014(7)	-0.0007(8)
M4	0.2482(4)	0.2101(1)	0.5004(2)	0.0135(4)	0.0166(9)	0.0110(9)	0.0134(8)	0.0001(7)	0.0034(7)	-0.0001(8)
As	0.0354(2)	0.57926(7)	0.70789(9)	0.0048(2)	0.0055(5)	0.0036(4)	0.0053(4)	0.0001(3)	0.0003(3)	0.0009(4)
O1	0.4480(2)	0.30627(9)	0.1151(1)	0.0076(2)	0.0084(6)	0.0071(5)	0.0076(5)	0.0001(4)	0.0013(4)	-0.0006(5)
O2	0.0603(2)	0.56991(9)	0.8786(1)	0.0067(2)	0.0082(5)	0.0063(5)	0.0055(4)	0.0004(4)	0.0001(4)	0.0001(5)
O3	0.0767(2)	0.84634(9)	0.9048(1)	0.0075(2)	0.0077(6)	0.0062(5)	0.0083(5)	-0.0003(4)	0.0001(5)	0.0006(5)
O4	0.9183(2)	0.70253(9)	0.6679(1)	0.0079(2)	0.0107(6)	0.0055(5)	0.0075(5)	0.0004(4)	0.0004(4)	0.0024(5)
O5	0.5771(2)	0.43729(9)	0.8866(1)	0.0075(2)	0.0088(6)	0.0050(5)	0.0087(5)	0.0004(4)	0.0003(4)	0.0002(5)
O6	0.5431(2)	0.18381(9)	0.3751(1)	0.0073(2)	0.0084(6)	0.0047(5)	0.0087(5)	0.0010(4)	-0.0005(4)	-0.0014(5)
O7	0.8522(2)	0.48012(9)	0.6384(1)	0.0070(2)	0.0081(5)	0.0052(5)	0.0074(5)	0.0002(4)	-0.0010(4)	-0.0019(5)
O8	0.3227(2)	0.57240(9)	0.6645(1)	0.0080(2)	0.0064(5)	0.0104(5)	0.0075(5)	-0.0019(4)	0.0017(4)	0.0001(5)
H1	0.5136(4)	0.3476(2)	0.1942(2)	0.0200(5)	0.0238(12)	0.0191(10)	0.0164(10)	-0.0044(9)	-0.0014(9)	-0.0027(9)
H3	0.1840(4)	0.8667(2)	0.8398(2)	0.0246(5)	0.0226(12)	0.0278(11)	0.0252(11)	0.0061(9)	0.0116(10)	-0.0002(10)
H5	0.5239(4)	0.4733(2)	0.8036(2)	0.0234(5)	0.0330(13)	0.0244(11)	0.0122(10)	0.0040(10)	-0.0005(9)	0.0020(10)
H6	0.6345(4)	0.2512(2)	0.3715(2)	0.0240(5)	0.0282(13)	0.0156(11)	0.0277(11)	0.0043(8)	0.0005(9)	-0.0103(10)

559 Table 4. Relevant bond distances (Å) and angles (°) based on the X-ray (XR) and
560 neutron (N) structure refinements for allactite at 293 K and 100 K.
561
562

T (K)	XR-293	N-293	N-100
M1-O3 x 2	2.1830(8)	2.152(1)	2.157(1)
M1-O8 x 2	2.2106(8)	2.182(1)	2.177(1)
M1-O7 x 2	2.3014(8)	2.278(1)	2.276(1)
<M1-O>	2.232	2.204	2.203
M2-O1	2.1152(8)	2.100(2)	2.100(2)
M2-O6	2.1469(8)	2.130(2)	2.129(2)
M2-O3	2.1435(9)	2.132(2)	2.136(2)
M2-O7	2.1541(8)	2.133(2)	2.134(2)
M2-O4	2.2223(8)	2.204(2)	2.202(2)
M2-O5	2.6151(9)	2.581(2)	2.574(2)
<M2-O>	2.233	2.213	2.212
M3-O6	2.1094(8)	2.089(2)	2.093(2)
M3-O5	2.1821(8)	2.166(2)	2.163(2)
M3-O5	2.1805(9)	2.160(3)	2.167(2)
M3-O1	2.1906(8)	2.171(2)	2.167(2)
M3-O2	2.2561(8)	2.243(2)	2.234(2)
M3-O2	2.2684(8)	2.249(2)	2.242(2)
<M3-O>	2.198	2.180	2.178
M4-O3	2.1143(8)	2.093(2)	2.095(2)
M4-O1	2.1242(8)	2.096(3)	2.104(2)
M4-O4	2.1362(8)	2.117(2)	2.122(2)
M4-O6	2.1777(9)	2.167(3)	2.163(2)
M4-O5	2.2955(8)	2.283(2)	2.276(2)
M4-O2	2.3121(8)	2.293(2)	2.285(2)
<M4-O>	2.193	2.175	2.174
As-O4	1.6783(8)	1.659(1)	1.664(1)
As-O7	1.6859(8)	1.669(2)	1.676(1)
As-O8	1.6826(9)	1.672(2)	1.675(1)
As-O2	1.7176(8)	1.701(1)	1.705(1)
<As-O>	1.691	1.675	1.680
O1-H1	0.93(1)	0.972(2)	0.977(3)
*O1-H1**		0.987	0.993
O1···O8		2.854(3)	2.842(2)
H1···O8		1.888(3)	1.871(3)
O1-H1···O8		172.0(2)	172.6(2)
O3-H3	0.88(1)	0.943(2)	0.951(2)
*O3-H3**		0.978	0.976
O3···O5		3.160(3)	3.155(2)
H3···O5		2.695(3)	2.699(3)
O3-H3···O5		111.2(2)	110.1(2)
O3···O6		3.676(3)	3.668(1)
H3···O6		2.822(3)	2.804(2)
O3-H3···O6		151.2(2)	151.5(2)
O3···O7		3.601(3)	3.589(2)
H3···O7		2.900(3)	2.880(3)
O3-H3···O7		132.1(2)	132.3(2)
O5-H5	0.88(1)	0.951(2)	0.959(3)
*O5-H5**		0.977	0.981
O5···O8		3.009(3)	2.996(2)
H5···O8		2.098(3)	2.075(3)
O5-H5···O8		159.9(2)	160.6(2)
O5···O7		3.071(3)	3.072(1)
H5···O7		2.553(3)	2.560(2)
O5-H5···O7		114.4(2)	113.6(2)
O5···O3		3.160(3)	3.155(2)
H5···O3		2.615(3)	2.610(2)
O5-H5···O3		116.8(2)	116.4(2)
O6-H6	0.92(1)	0.959(2)	0.963(3)
*O6-H6**		0.983	0.986
O6···O8		3.089(3)	3.088(2)
H6···O8		2.197(3)	2.190(3)
O6-H6···O8		154.3(2)	154.6(2)
O6···O4		3.336(3)	3.324(2)
H6···O4		2.587(3)	2.581(3)
O6-H6···O4		135.1(2)	134.1(2)

*Bond distance corrected for "riding motion" following Busing and Levy (1964).

563
564

Table 5. Positions and assignments of *d-d* bands and crystal field parameters for $^{VI}Mn^{2+}$ in allactite (see text for details).

ν (cm^{-1})	*M1*	*M2, M3, M4*
29020		$^6A_1(S) \rightarrow {}^4E_g(D)$
28675	$^6A_1(S) \rightarrow {}^4E_g(D)$	
27140	$^6A_1(S) \rightarrow {}^4T_{2g}(D)$	
26690		$^6A_1(S) \rightarrow {}^4T_{2g}(D)$
24470		$^6A_1(S) \rightarrow {}^4E_g{}^4A_{1g}(G)$
24180	$^6A_1(S) \rightarrow {}^4E_g{}^4A_{1g}(G)$	
22520	$^6A_1(S) \rightarrow {}^4T_{2g}(G)$	
21600		$^6A_1(S) \rightarrow {}^4T_{2g}(G)$
18810		$^6A_1(S) \rightarrow {}^4T_{1g}(G)$
17465	$^6A_1(S) \rightarrow {}^4T_{1g}(G)$	
B (cm^{-1})	642	650
C (cm^{-1})	3552	3594
10*Dq* (cm^{-1})	8811	8948

Figure 1. Clinographic view of the crystal structure of allactite (H-free structure model), using the reduced cell with $a \approx 5.5$ Å, $b \approx 12.1$ Å, $c \approx 10.1$ Å and $\beta \approx 95.7°$, space group $P2_1/n$. The reduced cell can be obtained from the non-reduced cell choice of Moore (1968) with $a \approx 11.0$ Å, $b \approx 12.1$ Å, $c \approx 5.5$ Å and $\beta \approx 114.1°$, space group $P2_1/a$, by the transformation [001/010/-10-1].

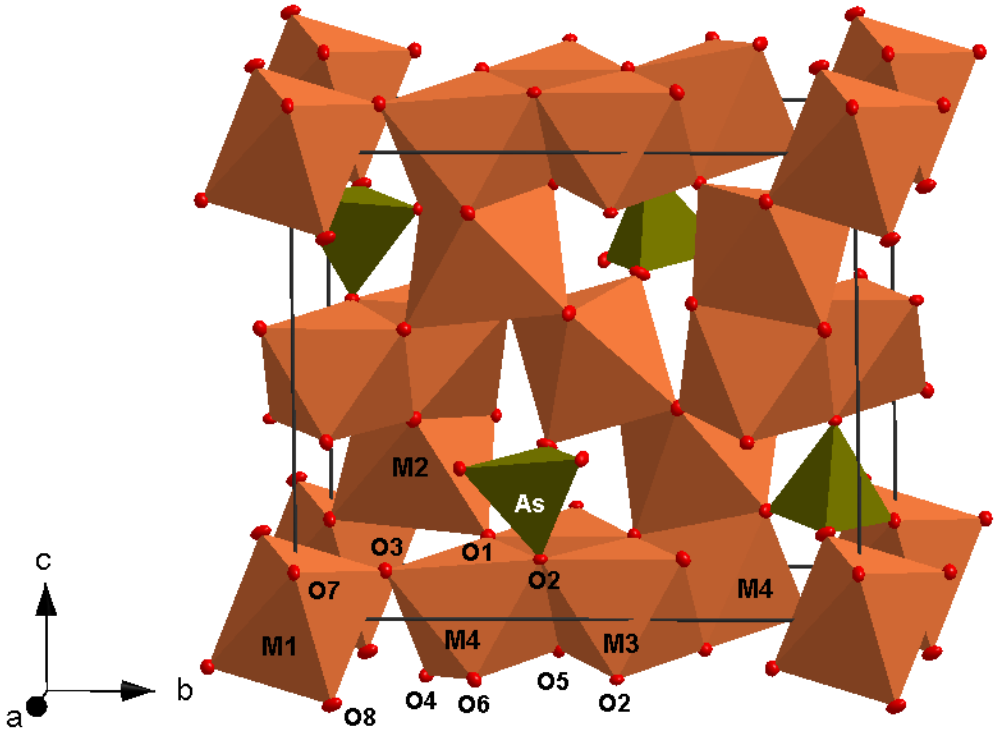

Figure 2. Polarized optical absorption spectra of allactite.

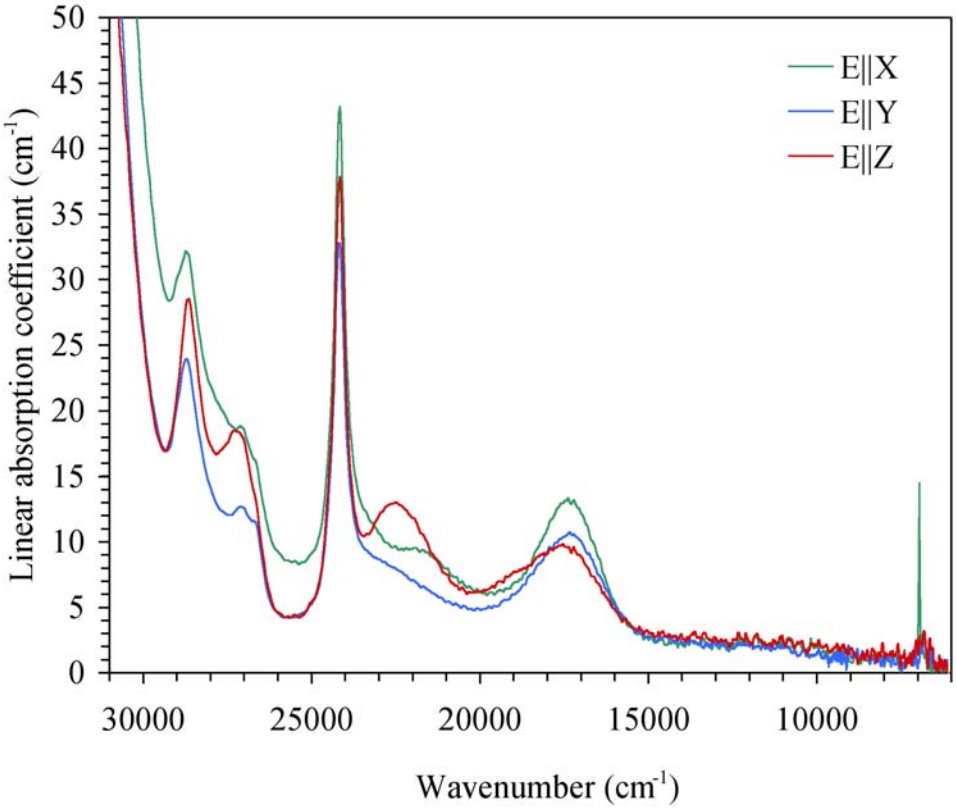

Figure 3. FTIR-spectrum of allactite in the region 3900 – 2900 cm^{-1}.

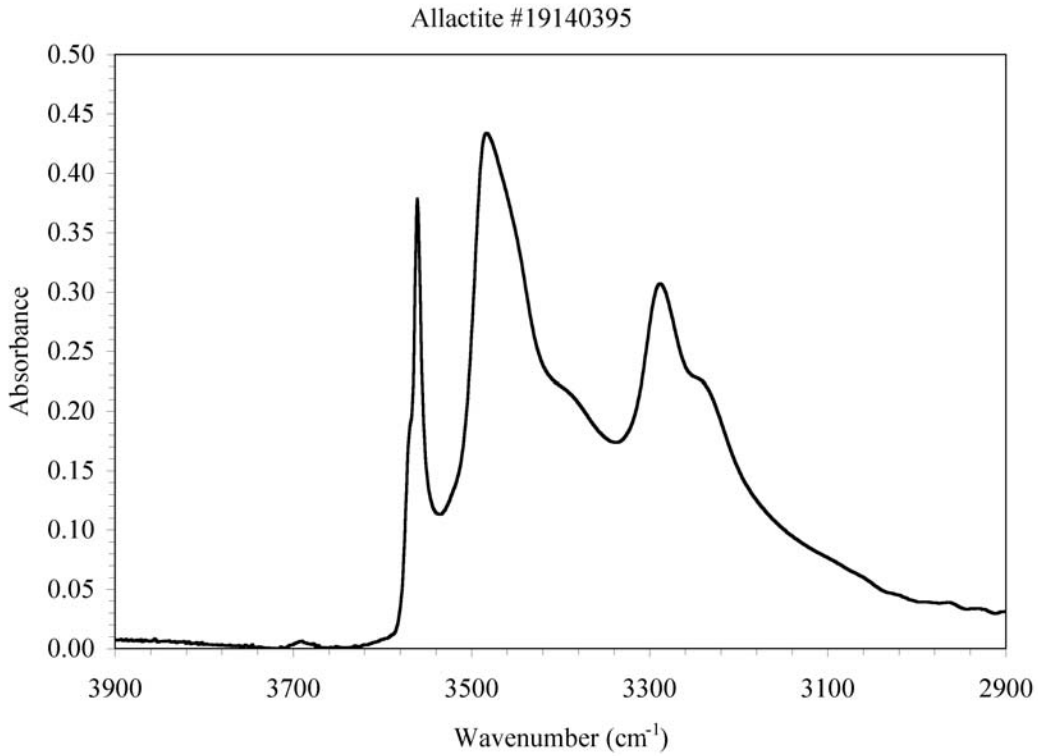

Figure 4. The H-bonding scheme in allactite, based on the neutron structure refinement of this study (at 293 K). Displacement ellipsoids probability factor: 50%.

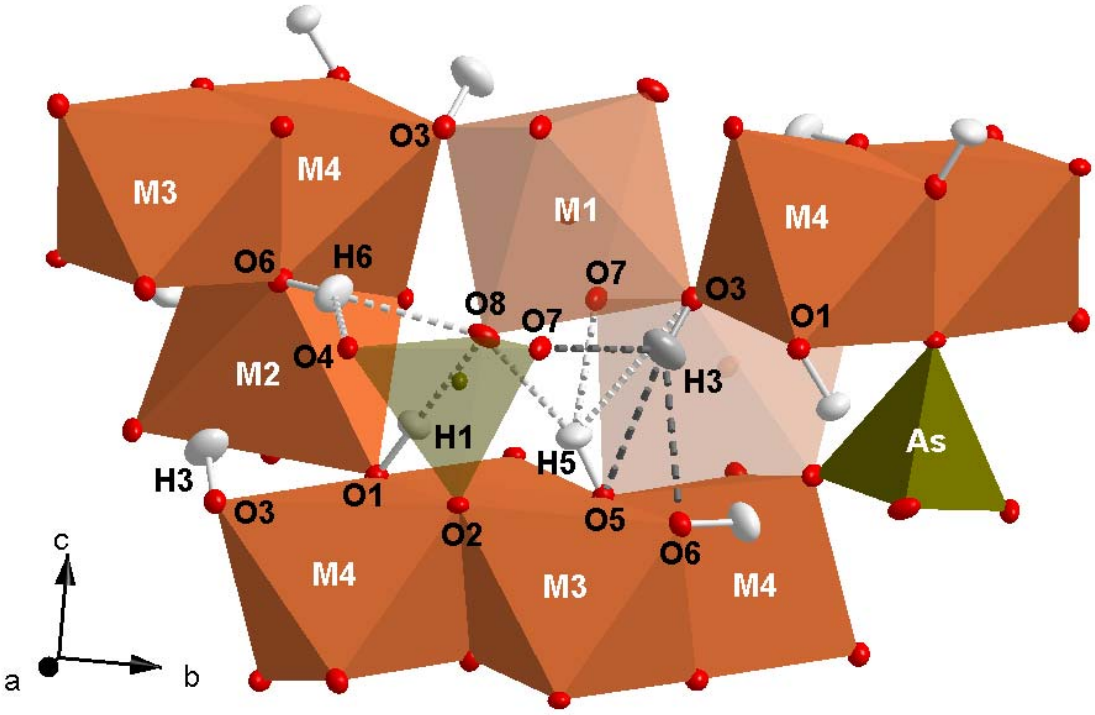

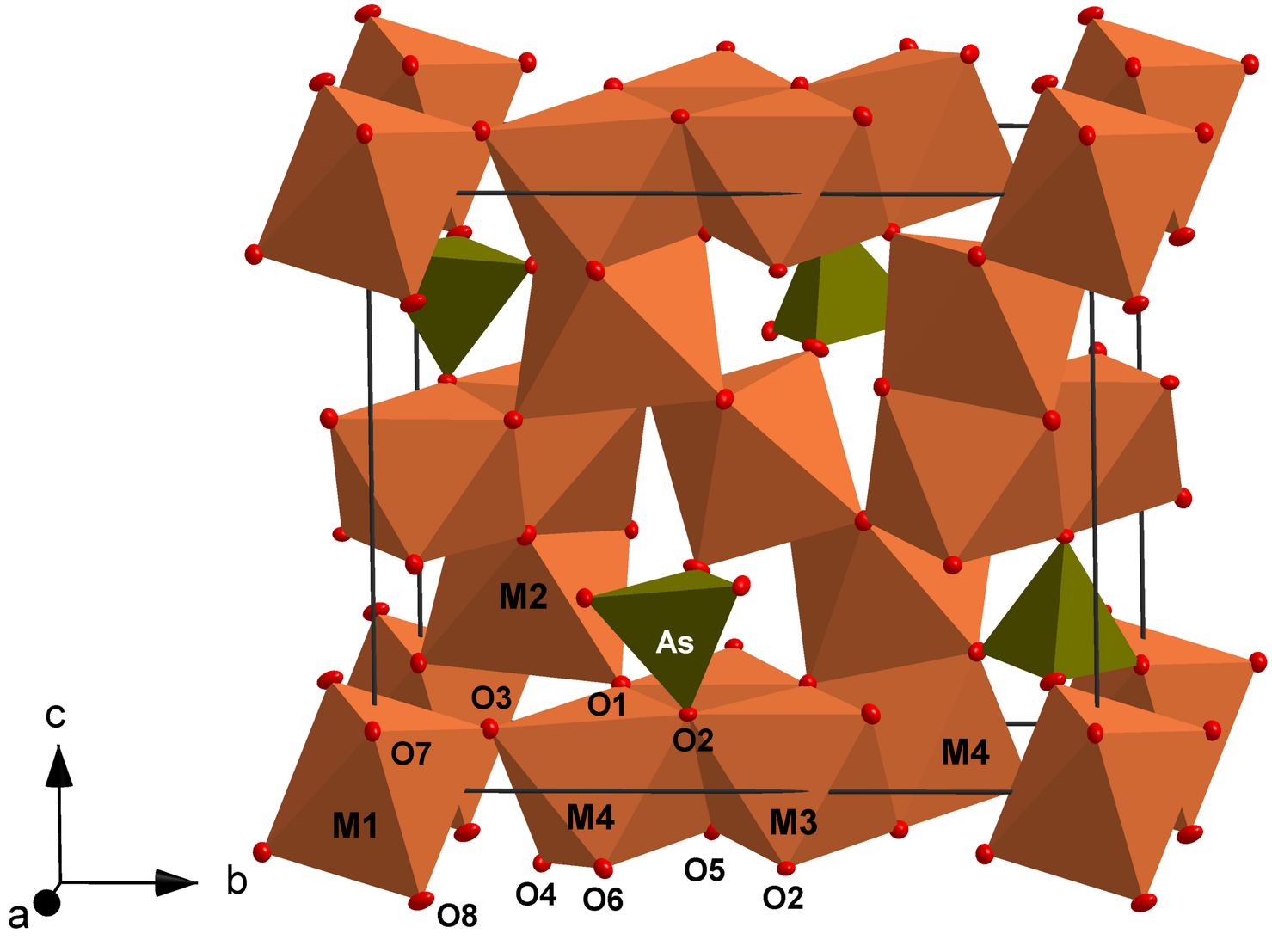
c
b
a
M2
As
O3
O1
O2
O7
M4
M1
M4
M3
O5
O4
O6
O2
O8

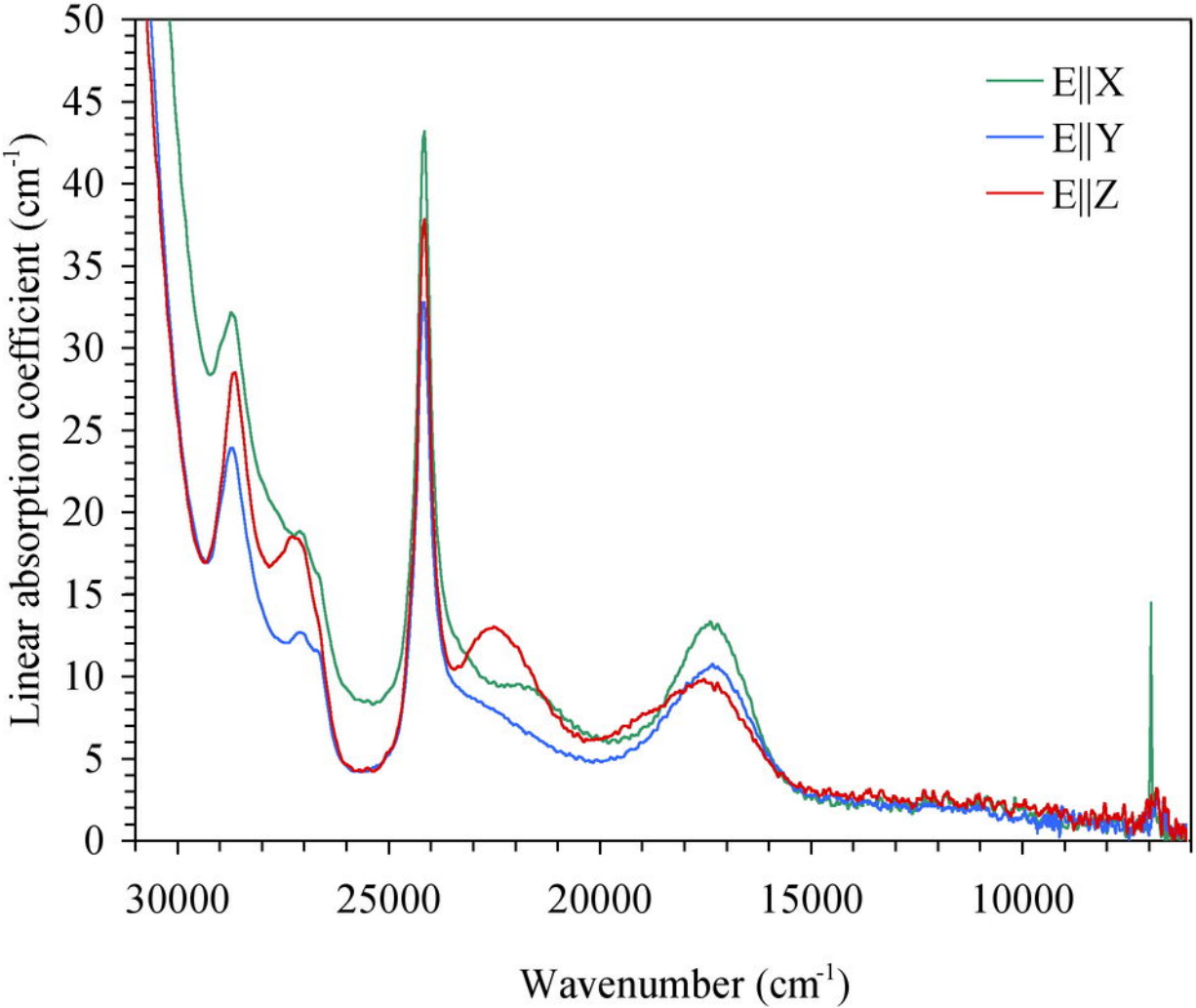
E||X
E||Y
E||Z
Linear absorption coefficient (cm-1)
Wavenumber (cm-1)
0
5
10
15
20
25
30
35
40
45
50
30000
25000
20000
15000
10000

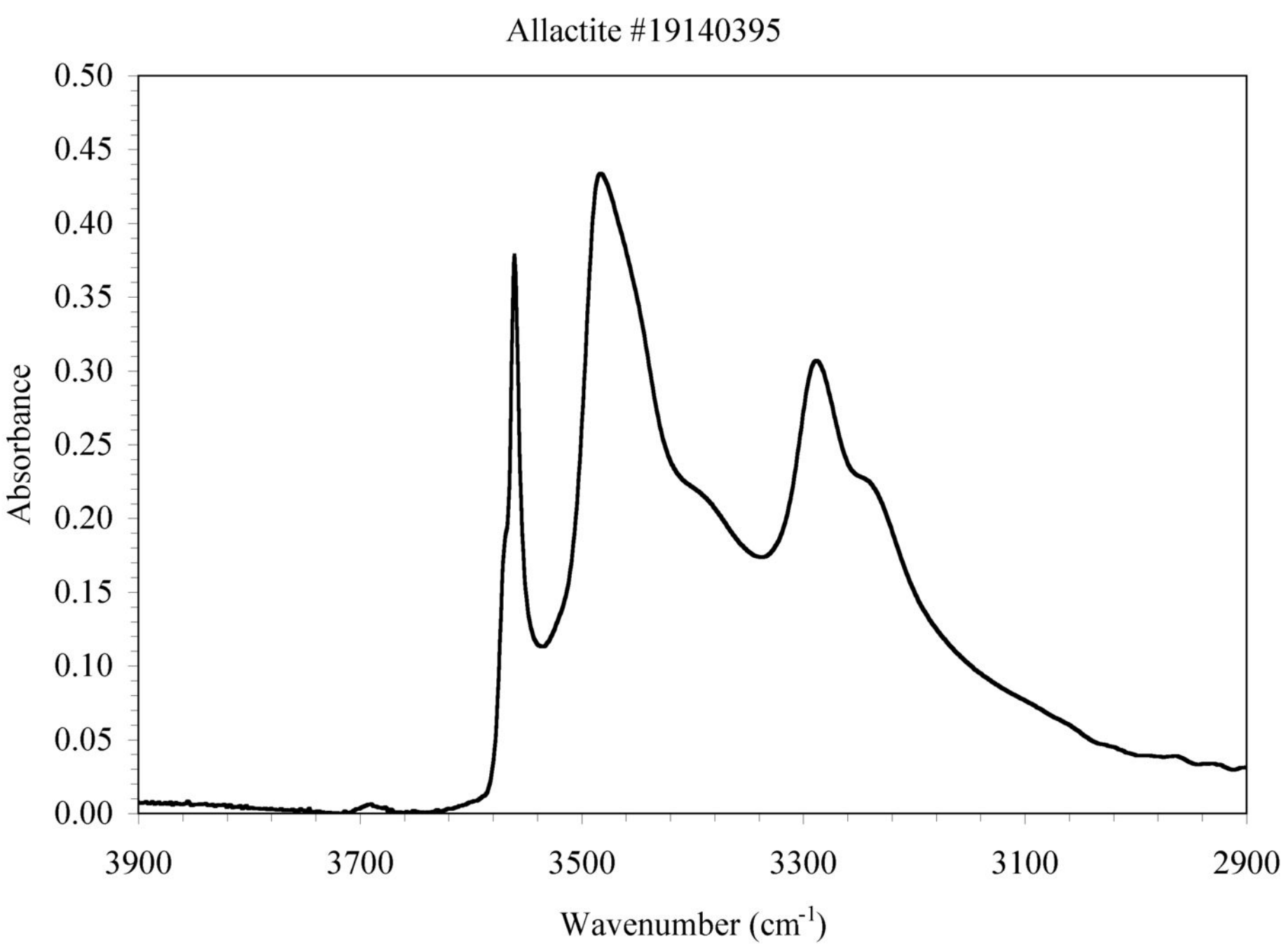
Allactite #19140395
0.50
0.45
0.40
0.35
0.30
0.25
0.20
0.15
0.10
0.05
0.00
Absorbance
3900
3700
3500
3300
3100
2900
Wavenumber (cm-1)

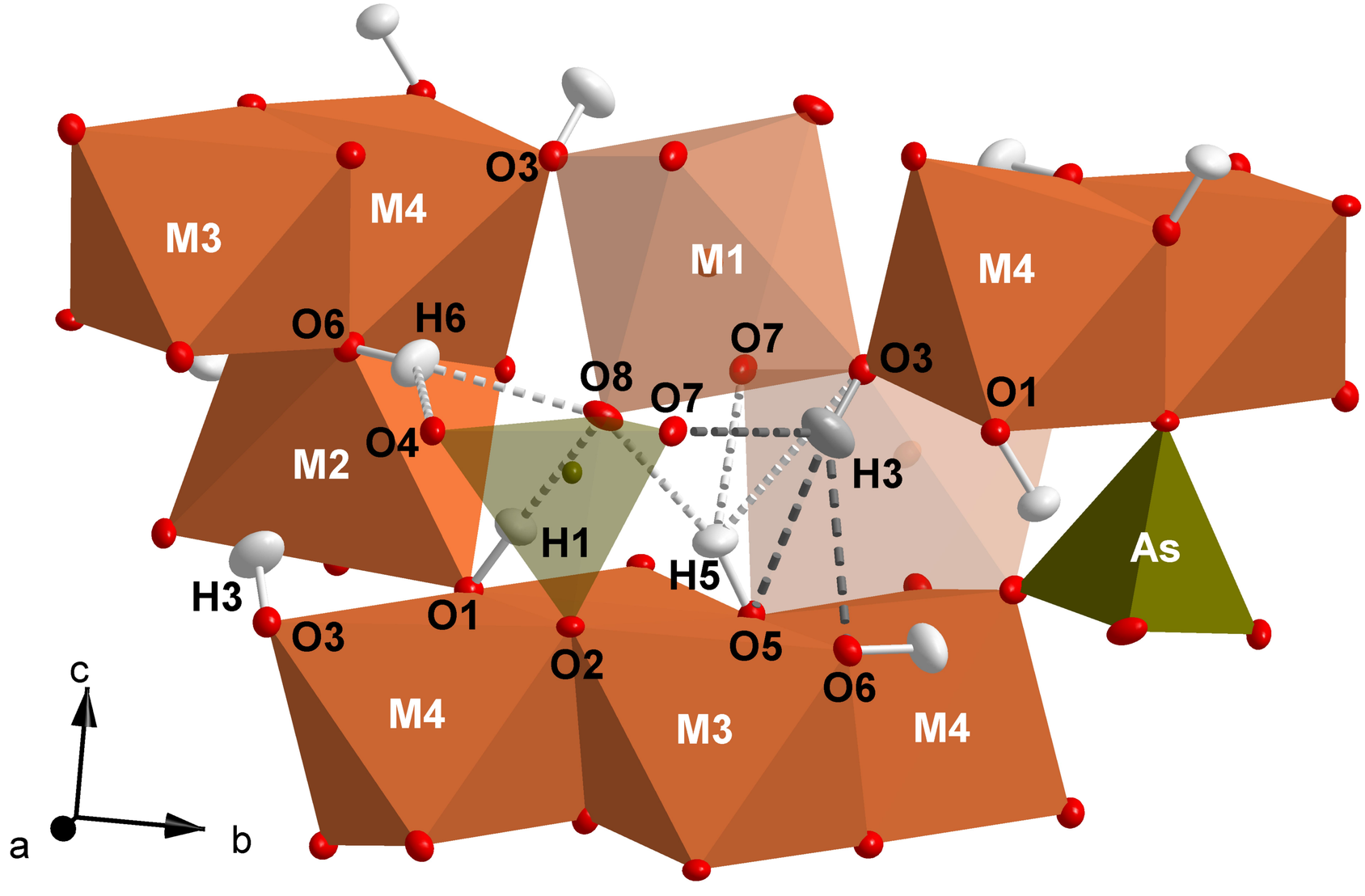
M3
M4
O3
M1
M4
O6
H6
O7
O3
O8
O7
O1
O4
M2
H3
H1
H5
As
H3
O3
O1
O2
O5
O6
M4
M3
M4
c
a
b